THE JOURNAL OF PHYSICAL CHEMISTRY A
A JOURNAL OF THE AMERICAN CHEMICAL SOCIETY

pubs.acs.org/JPCA

Article

Influence of Transition Metal Electron Configuration on the Structure of Metal−EDTA Complexes

Madison M. Foreman, Maristella Alessio, Anna I. Krylov, and J. Mathias Weber*

Cite This: J. Phys. Chem. A 2023, 127, 2258−2264

Read Online

ACCESS | Metrics & More | Article Recommendations | Supporting Information

ABSTRACT: The vibrational spectra of cold complexes of ethylenediaminetetraacetic acid (EDTA) with transition metal dications in vacuo show how the electronic structure of the metal provides a geometric template for interaction with the functional groups of the binding pocket. The OCO stretching modes of the carboxylate groups of EDTA serve as structural probes, informing on the spin state of the ion as well as the coordination number in the complex. The results highlight the flexibility of EDTA in accepting a large range of metal cations in its binding site.

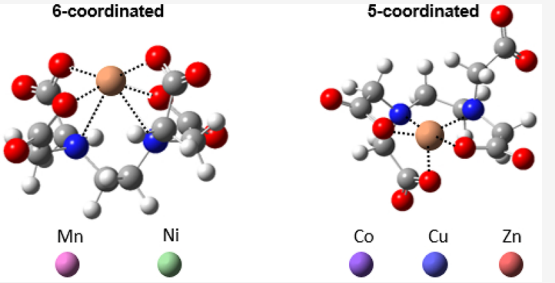

INTRODUCTION

Supramolecular structures that can bind metal cations are important in a broad range of chemical scenarios, including binding sites in metalloenzymes,[1] sensing of metal ions,[2] the effective removal of metal cations (to decrease their toxicity[3]), and ionophores for flow batteries.[4] Ethylenediaminetetraacetic acid (EDTA) is a widely used chelator for metal cations, forming a binding pocket generated by its two N atoms and four COO^- groups (see Figure 1). It has a remarkably high affinity for nearly all metal cations in the periodic system,[5] and it is frequently used as an enzyme inhibitor for metalloenzymes.[6]

The near-universal ability of EDTA to accommodate metal cations comes from its molecular flexibility, which allows it to respond to the chemical nature of the metal ion it binds. As a consequence, one expects the geometry of the binding pocket around a given ion to be a function of ion size[7] but also dependent on the electronic structure of the metal ion itself. For example, while alkaline earth dications present to their chemical environment as simple, spherically symmetric charge distributions, transition metal ions structure their environment through the occupation of their d-orbitals. In many transition metal complexes, the structural template of the electronic structure of the metal ion even dominates the structure of the ligand frame around the metal ion.

In the condensed phase, the environment (e.g., protein or solvent) influences the interactions of ions with ion receptors and chelators such as EDTA.[7−9] In addition, the presence of solvent molecules can mask the spectroscopic response of the complex under study, and the spectroscopic signatures can be rather broad.[7,9] Experiments on mass-selected ions circumvent many of these problems, allowing one to gauge the intrinsic interactions between the ion and the chelator. Cryogenic preparation of the target ions serves to further simplify their spectroscopic response. In pioneering work, Wang and coworkers[10,11] concluded on the basis of photoelectron spectra and density functional theory (DFT) calculations of divalent first-row transition metal complexes with EDTA that all complexes adopt a hexacoordinated structure. However, they attributed pentacoordinated conformations to Cu(II)-EDTA complexes as well, and they recognized that the coordination number of the bound metal ion could, in principle, vary from four to six.

In the present work, we use cryogenic ion vibrational spectroscopy (CIVS) and DFT calculations to characterize the ion−chelator interactions for complexes of selected divalent transition metal ions M^{2+} (M = Mn, Co, Ni, Cu, and Zn).

METHODS

Experimental Section. Solutions of $[M(II)\cdot EDTA]^{2-}$ (M = Mn, Co, Ni, Cu, and Zn) were prepared by first making 5 mM stock solutions in water with EDTA and the corresponding metal salt ($MnCl_2$, $CoCl_2$ or $Co(NO_3)_2\cdot(H_2O)_6$, $Cu(NO_3)_2\cdot(H_2O)_3$, $ZnCl_2$, and $Ni(NO_3)_2(H_2O)_3$). All chemicals were used without further purification. Aliquots of stock solution were diluted with acetonitrile to 0.3−1 mM and electrosprayed. Solutions of Mn(II) ions and EDTA were adjusted to pH 5 using KOH and HCl to optimize ion production. Similarly, solutions of EDTA with Zn(II) and Ni(II) were adjusted to pH = 8−12. We note that we were

Received: November 14, 2022
Revised: January 23, 2023
Published: March 6, 2023

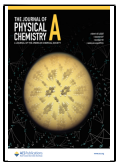

https://doi.org/10.1021/acs.jpca.2c07996
J. Phys. Chem. A 2023, 127, 2258−2264

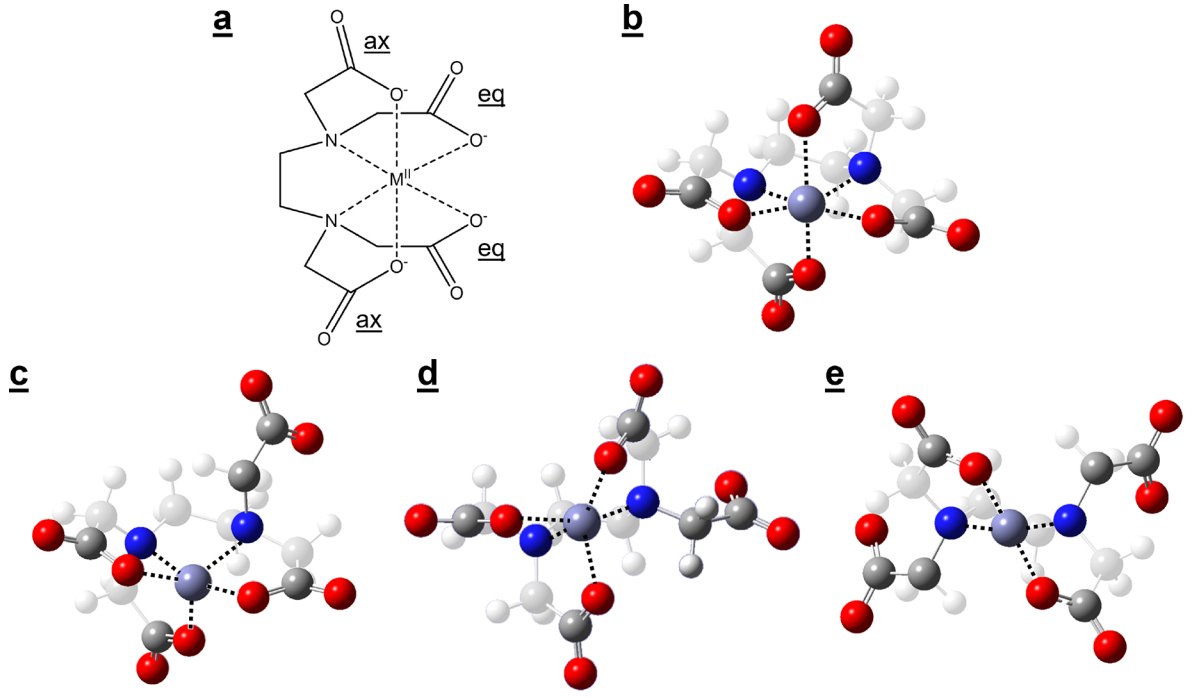

Figure 1. Structure of EDTA complexes with metal dications. (a) $[M(II)\cdot EDTA]^{2-}$ line drawing; equatorial and axial ligands are labeled "eq" and "ax", respectively. (b–e) Calculated ball-and-bond-type structures of $[M(II)\cdot EDTA]^{2-}$ complexes in hexa- (b), penta- (c, d), and tetracoordinated (e) geometries using M = Zn as an example. Pentacoordinated structures can have an axial (c) or equatorial ligand (d) detached from the metal center. The metal environment in the tetracoordinated structures (e) is approximately tetrahedral, making such distinctions less useful. Carbon atoms are shown in gray, hydrogen in white, nitrogen in blue, oxygen in red, and the central metal atom in blue-gray. Dotted lines show the coordination of the metal atom. The parts of the EDTA molecule that are not part of the binding pocket are shown in lighter gray tones.

unable to generate analogous Fe(II) complexes. This problem has been commented on by Wang and co-workers,[11] who attributed the difficulty of electrospraying $[Fe(II)\cdot EDTA]^{2-}$ to oxidation during the electrospray process and hypothesized that these complexes may not be electronically stable.

The setup for CIVS has been described in detail in earlier work.[12] Briefly, solutions prepared as described above were electrosprayed to produce $[M(II)\cdot EDTA]^{2-}$ ions, which entered a heated desolvation capillary. After passing through a skimmer, the ions were guided through a series of differentially pumped octopole guides into a Paul trap, which was kept at 30 K using a closed-cycle He cryostat. The ions were cooled in the trap by collisions with buffer gas. The buffer gas is predominantly D_2 but also contains a small amount of N_2 that enters the apparatus through the electrospray source and is part of the background gas in the chamber. During the cooling time, weakly bound complexes with N_2 molecules were formed. The contents of the ion trap were injected into the acceleration region of a time-of-flight mass spectrometer with a repetition rate of 20 Hz. Target ions of the form $[M(II)\cdot EDTA]^{2-}\cdot N_2$ were mass-selected using an interleaving comb mass gate and subsequently irradiated with the output of an optical parametric converter (bandwidth, ca. 2 cm^{-1}; pulse duration, 5–7 ns) tuned throughout the IR fingerprint region (range covered here, 1200–1750 cm^{-1}). Absorption of single IR photons results in the loss of the N_2 adduct. The resulting $[M(II)\cdot EDTA]^{2-}$ fragment ions are separated from the undissociated parent ions in a two-stage reflectron, and the fragment ion intensity is monitored using a dual microchannel plate detector and normalized by the photon fluence to create a photodissociation spectrum. We note that the presence of N_2 tags has a negligible influence on the position of the vibrational modes in most cases.[13] Exploratory calculations for the present work estimate shifts on the order of 2 cm^{-1} for the antisymmetric OCO stretching vibrations of EDTA (see Computational Section for methods used here).

The laser is operated at 10 Hz repetition rate to allow the subtraction of background fragment signals due to unimolecular decay or collision-induced fragmentation. Signals were averaged over 16 laser shots for each wavelength in each scan, and several scans taken on different days were used for each ion species. The frequency of the optical parametric converter system was calibrated using a photoacoustic spectrum of acetone.[14]

Computational Section. Structures, adiabatic gaps, and IR spectra of the hexacoordinated $[M(II)\cdot EDTA]^{2-}$ ions under study were calculated in the framework of density functional theory (DFT) using two hybrid functionals (B3LYP[15,16] and B5050LYP[17]) and one long-range corrected hybrid DFT with empirical dispersion (ωB97X-D[18]). Scaled B3LYP, B5050LYP, and ωB97xD functionals provided similar-quality description of the main features in the spectra with respect to experiment. We selected ωB97xD for additional calculations on low-spin states and other isomers since range-separated functionals such as ωB97xD have shown robust performance in treating transition-metal compounds[19] and have shown a better accuracy for a variety of properties than lower-rung hybrid functionals.[20] To investigate penta- and tetracoordinated isomers, we therefore used the ωB97X-D functional only. Structures were obtained after minimization on the corresponding potential energy surface. We started with guess structures taken from previous DFT work.[11] Additional pentacoordinated structures were generated where an equatorial ligand instead of an axial ligand was detached

https://doi.org/10.1021/acs.jpca.2c07996
J. Phys. Chem. A 2023, 127, 2258–2264

from the metal center (see Figure 1d). We used def2-TZVPP basis sets[21] for all atoms to be consistent with previous work[7] on $[Ca(II)\cdot EDTA]^{2-}$. These calculations were performed using the Q-Chem electronic structure package.[22,23] Table S1 lists adiabatic energy gaps between high- and low-spin states for Mn, Co, and Ni compounds.

For the comparison with experiment, we used only results based on ωB97X-D. All frequencies were scaled by 0.950 to match the most intense feature of the antisymmetric OCO stretching region in $[Ca(II)\cdot EDTA]^{2-}$. All computational spectra were broadened by a Lorentzian with 8 cm^{-1} full width at half-maximum.

Additionally, for $[Mn(II)\cdot EDTA]^{2-}$, to screen the spectrum of its low-lying spin states, we performed spin-flip time-dependent (SF-TD)-DFT calculations[17] (using B5050LYP and a noncollinear kernel[24,25]), which yielded sextet and quartet spin states. Results are reported in Table S2. Spin contamination is small (within 0.02). Both adiabatic gaps (Table S1) and vertical excitation (Table S2) between high- and low-spin states are large, with the high-spin state being the lowest in energy. Frontier natural orbitals of the target sextet state obtained by SF-TD-DFT (Figure S1) indicate that unpaired electrons are well localized on the metal center.

Simulations of the complexes in solution were carried out using a polarizable continuum model[26] with the dielectric constant of water (78.36), the ωB97X-D functional, and def2-TZVP basis sets for all atoms,[21] employing Gaussian 16.[27]

RESULTS AND DISCUSSION

Figure 2 shows the experimental infrared (IR) signatures of $[M(II)\text{-}EDTA]^{2-}\cdot N_2$ complexes in the fingerprint region of the spectrum. There are two regions of interest, a lower frequency range (1300−1400 cm^{-1}) and a higher frequency range (1600−1700 cm^{-1}), containing IR signatures belonging predominantly to the OCO stretching modes of the carboxylate groups of EDTA. The lower frequency range mainly contains the signatures of linear combinations of the symmetric OCO stretching vibrations, while linear combinations of the antisymmetric stretching motions are found in the higher frequency range.

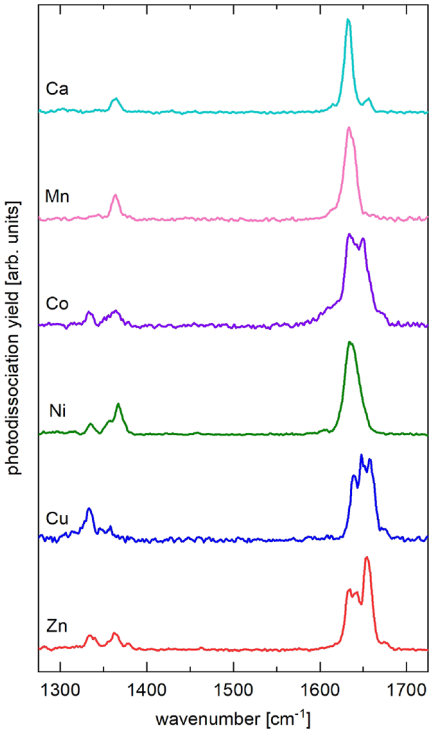

Figure 2. Experimental IR spectra of $[M(II)\text{-}EDTA]^{2-}\cdot N_2$ complexes in the fingerprint region (from top to bottom: M = Ca, Mn, Co, Ni, Cu, and Zn; metal identity given in each trace). Data for M = Ca taken from ref 7.

The spectrum of $[Ca(II)\text{-}EDTA]^{2-}$ provides the starting point for our discussion. As described previously,[7,9] this is a complex with C_2 symmetry, where the metal ion is hexacoordinated by the EDTA binding pocket. The antisymmetric OCO stretching motions of the EDTA moiety form four linear combinations, which give rise to partially resolved features in the higher frequency range. The feature at 1656 cm^{-1} represents the radial all-in-phase linear combination of the local OCO antisymmetric stretching motions, while the strong peak at 1632 cm^{-1} contains two unresolved modes, each pairing the motions of one equatorial ligand and one axial ligand. The shoulder at 1615 cm^{-1} is the signature of a mode that combines the motions of equatorial ligands radially in phase, with the axial ligands opposite in phase (see Figure S2 and ref 7). The peak at 1365 cm^{-1} contains the four unresolved analogous vibrational modes consisting of linear combinations of the symmetric OCO stretching vibrations.

For transition-metal complexes with EDTA, the patterns in the regions of the symmetric and antisymmetric stretching vibrations vary with the identity of the ion. For example, although the patterns for Ca and Mn complexes appear very similar in their simplicity, the spectrum of $[Mn(II)\cdot EDTA]^{2-}$ does not show significant intensity for the highest frequency component of the antisymmetric OCO stretching modes, which is clearly observed in the Ca complex. Most strikingly, the symmetric stretching patterns for M = Co, Ni, Cu, and Zn and the antisymmetric stretching modes for M = Co, Cu, and Zn show a considerably different substructure than the alkaline earth metal complexes.[7]

Since these patterns depend on the interaction of the metal ion with the carboxylate groups of the EDTA pocket, the electronic structure of the metal ions plays a key role in the spectroscopic properties. For M = Mn, Co, and Ni, different spin states of the metal ion are possible. Corroborating earlier results by Wang and co-workers,[11] our DFT calculations predict that the high-spin states are the lowest in energy in each case (see Table S1), and judging from the natural orbital analysis, the unpaired electrons are localized on the metal center (Figure S1). The match of the computed high-spin and experimental IR spectra is generally quite good (Figure 3). For M = Mn, the symmetric stretching region is recaptured better by the predicted spectrum of the sextet state. Similarly, for M = Ni, the predicted pattern of antisymmetric stretching modes clearly allows identification of the triplet state as a better fit to the experimental spectrum. Both of these cases independently corroborate photoelectron spectroscopy and computational results assigning the high-spin states to $[M(II)\cdot EDTA]^{2-}$ complexes.[11] For M = Co, the IR spectrum does not serve to uniquely identify the spin state, but based on the relative energies of the different states, we assume that the experimental IR spectrum belongs to the quartet state. The peculiar substructure of the antisymmetric stretching bands therefore cannot be explained by the presence of different spin states but has structural reasons, as will be explained below.

https://doi.org/10.1021/acs.jpca.2c07996
J. Phys. Chem. A 2023, 127, 2258−2264

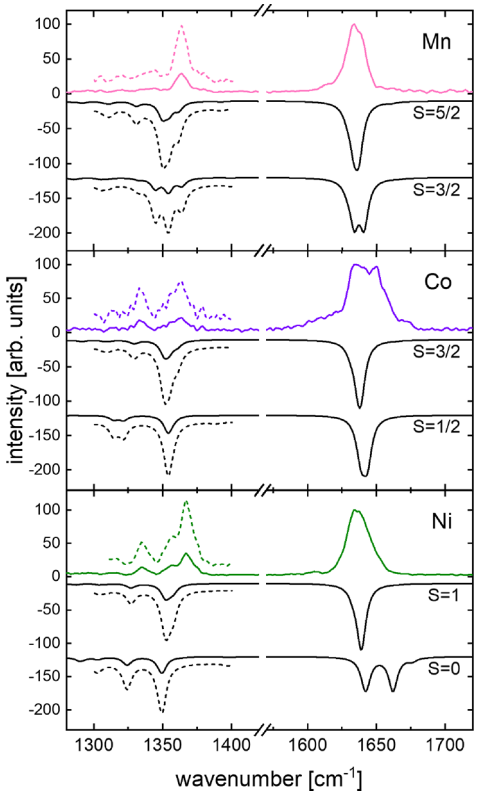

Figure 3. Experimental IR spectra of $[M(II)\text{-}EDTA]^{2-}\cdot N_2$ complexes (from top to bottom: M = Mn, Co, and Ni; metal identity given in each panel; spin, *S*, shown for each calculated trace) in comparison with DFT (ωB97X-D/Def2-TZVPP) calculations for hexacoordinated structures with different spin states. The calculated frequencies were scaled by 0.950 to match the signature of the main antisymmetric OCO stretching feature for $[Ca(II)\cdot EDTA]^{2-}$.[7] The dashed lines represent experimental and computed intensities multiplied by 3. The experimental spectra are shown in a color that varies with the identity of the metal ion, while the calculated spectra are shown in black. The intensities of the calculated spectra for high-spin complexes are scaled to fit the antisymmetric stretching region in each experimental spectrum. The relative intensities of low-spin and high-spin complexes are to scale.

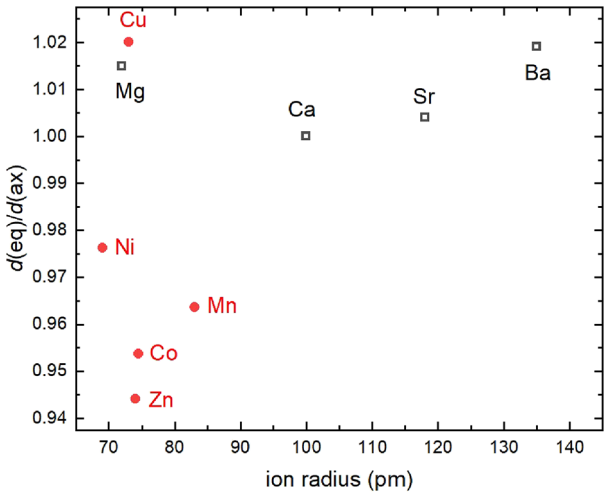

Figure 4. Calculated aspect ratio of equatorial to axial metal−oxygen bond distances (see Table S3) as a function of ion radius for different divalent metal cations. Open squares show the data for alkaline earth metals,[7] while filled circles show data for the transition metals under study in the present work.

The influence of the electronic structure on the IR patterns can be rationalized by the population of d-orbitals in the metal ion and the resulting structural differences between the different complexes. In particular, the different d-orbital occupations result in differences in the calculated distances of the metal ion to the closest O atoms for equatorial and axial ligands in the EDTA binding pocket (see Table S3). This difference in interaction strength results in Jahn−Teller-like distortions of the coordination environment and is reflected in the ratio of the equatorial and axial metal−oxygen distances, d_{eq} and d_{ax}, respectively (see Figure 4). For the alkaline earth metals with their spherical charge distribution,[7] this ratio is in a narrow band around 1.01, with deviations from this value of only 0.01, despite the large disparity in ion radius. For the transition metal ions studied in the present work, the range of values of this ratio is much larger, showing the significant difference in interactions between equatorial and axial ligands, even though the ion radii are rather similar for the ions studied here. As a result, the kinematic coupling between the local OCO stretching oscillators with similar frequencies changes, and the participation of the individual carboxylate groups in each mode as well as the frequencies of each mode changes as well (Table S4).

Within the hexacoordinated structures of $[M(II)\cdot EDTA]^{2-}$ complexes, the predicted overall pattern in the antisymmetric stretching region remains simple, with little structure that would be resolvable in our experiment. However, the antisymmetric stretching region shows a complex substructure for M = Co, Cu, and Zn. Wang and co-workers[11] proposed that the complexes for these metal ions could be penta- or even tetracoordinated rather than hexacoordinated (see Figure 1). Figure 5 shows the experimental IR spectra for M = Co, Cu, and Zn compared to the simulated IR spectra for different coordination isomers. The predicted IR patterns in the antisymmetric stretching region blue-shift significantly for decreasing coordination numbers of the metal ion. Somewhat different from the results of Wang and co-workers, who assigned their photoelectron spectra mostly to hexacoordinated structures,[11] we find the pentacoordinated structures in all three cases to be practically isoenergetic with the hexacoordinated structures (see Table 1). However, the differences in the energies calculated by Wang and co-workers and in the present work are small. Their relative energies for pentacoordinated Co, Cu, and Zn are quite low,[11] and the differences between the different computational results do not represent a drastic disagreement. We note that the spectral congestion in the photoelectron spectra reported by Wang and co-workers[11] does not allow to exclude the presence of pentacoordinated complexes.

Wang and co-workers[11] calculated the barriers between hexa- and pentacoordinated isomers to be around 1 eV, except for M = Cu (0.29 eV), so the thermal occupation probability of different isomers at cryogenic temperatures can be neglected. However, these complexes are formed from solutions at room temperature, where the thermal energy content of $[M(II)\cdot EDTA]^{2-}$ complexes can be estimated at ca. 0.5 eV, and they may suffer energetic collisions in the first stages of the electrospray source. They may also adopt a pentacoordinated structure in solution, which could persist in the gas phase, although our calculations using a polarizable continuum model indicate that penta- and tetracoordinated isomers in aqueous

https://doi.org/10.1021/acs.jpca.2c07996
J. Phys. Chem. A 2023, 127, 2258−2264

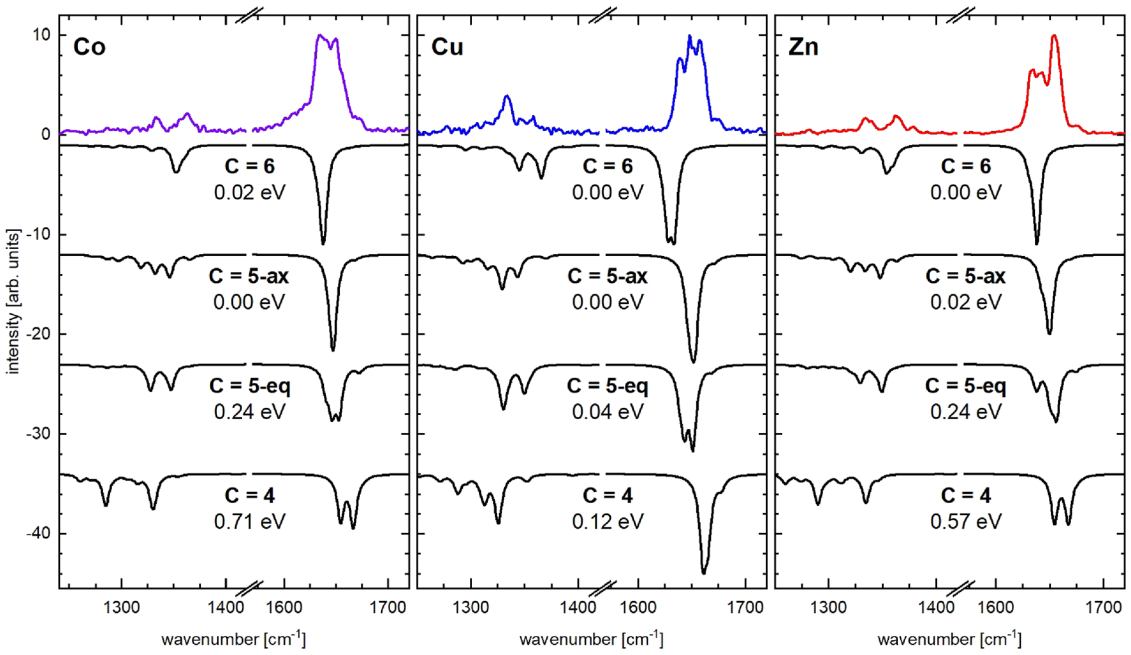

Figure 5. Experimental IR spectra of $[M(II)\text{-}EDTA]^{2-}\cdot N_2$ complexes (from left to right: M = Co, Cu, and Zn; metal identity given in each panel; coordination number, *C*, shown for each calculated trace) in comparison with DFT (ωB97X-D/Def2-TZVPP) calculations for different coordination numbers of the EDTA binding pocket (high-spin complexes only). The experimental spectra are shown in a color that varies with the identity of the metal ion, while the calculated spectra are shown in black. The intensities of the calculated spectra for hexacoordinated complexes are scaled to fit the antisymmetric stretching region in each experimental spectrum. The relative intensities for *C* = 4, 5, and 6 are to scale.

Table 1. Relative Energies (Zero Point-Corrected, in eV) of $[M(II)\cdot EDTA]^{2-}$ Isomers with Different Coordination Numbers Using ωB97X-D/Def2-TZVPP

coordination	Mn[a]	Co[a]	Ni[a]	Cu	Zn
6	0	0.02	0	0	0
5 (ax/eq)[b]	0.27/0.44	0/0.24	0.21/0.25	0/0.04	0.02/0.24
4	1.09	0.71	0.64	0.12	0.57

[a]Only the high-spin state for each metal was used. [b]The first number is for an axial ligand detached from the metal and the second for a detached equatorial ligand.

solution are significantly (more than ca. 200 meV; see the Supporting Information) higher in energy than the hexacoordinated structures, rendering pentacoordinated structures in solutions less likely. Rapid cooling in the cryogenic ion trap can kinetically freeze ionic species in structures at higher energies. In view of these arguments, we explain the rich substructure in the spectra of $[Co(II)\cdot EDTA]^{2-}$, $[Cu(II)\cdot EDTA]^{2-}$, and $[Zn(II)\cdot EDTA]^{2-}$ with coexisting hexa- and pentacoordinated isomers. For M = Zn, this is consistent with work by Williams and co-workers[28,29] who showed that the Zn^{2+} ion prefers 5-fold coordination in hydrated cluster ions. For M = Cu, structures with axial or equatorial ligands detached from the metal center are likely to contribute based on the energies shown in Table 1. While the isomers with detached equatorial ligands found in our calculations tend to be higher in energy for the other metals, we note that the potential energy landscapes for the pentacoordinated isomers are complex and may allow for the existence of additional structures. The presence of pentacoordinated structures also explains the small shoulders at ca. 1675 cm^{-1} on the high-energy side of the antisymmetric OCO stretching region. They are present as weak features in the calculated spectra of the pentacoordinated complexes but not in those of the hexacoordinated structures. For $[Cu(II)\cdot EDTA]^{2-}$, small contributions of tetracoordinated isomers could also contribute to the spectrum, but we exclude those based on their high relative energies for all other metals (see Table 1).

Even $[Ni(II)\cdot EDTA]^{2-}$ may not exclusively be hexacoordinated. Although its spectrum presents only one peak in the OCO antisymmetric region, this feature is sufficiently broad (full width at half-maximum, ca. 20 cm^{-1}) that it may encompass a minor contribution from the high-energy peak of the pentacoordinated structure with a detached axial COO^- group (see the Supporting Information). The simulated IR spectrum of this isomer also captures portions of the pattern in the symmetric stretching region. In contrast, the analogous feature observed for $[Mn(II)\cdot EDTA]^{2-}$ is unlikely to represent more than the hexacoordinated structure, as the other calculated spectra did not produce peaks within the envelope of the experimental band (see the Supporting Information). While the spectral congestion in the region of the antisymmetric OCO stretching modes prevents a quantitative identification of the contribution of each isomer, the intensity variation allows us a qualitative assessment. The envelope of the antisymmetric OCO stretching modes shifts to blue with decreasing coordination. For $[Co(II)\cdot EDTA]^{2-}$, the roughly equal intensity distribution in the lower and higher frequency features in this region suggests that hexa- and pentacoordinated structures have similar populations, while the ratio of penta- to hexacoordinated populations is higher for $[Cu(II)\cdot EDTA]^{2-}$ and higher still for $[Zn(II)\cdot EDTA]^{2-}$. This is not completely reflected by the calculated energy differences, but these differences are rather small, and Boltzmann-weighted populations do not accurately describe kinetic trapping in different parts of the potential energy landscape, which may be at play here.

https://doi.org/10.1021/acs.jpca.2c07996
J. Phys. Chem. A 2023, 127, 2258−2264

We note that the conformational variations and the differences observed for the different metal centers may be influenced by metal-specific Jahn–Teller-like distortions, charge transfer to the metal center (see the Supporting Information), which affects the local electronic structure, and electrostatic constraints of the chelating ligand—all of which are encoded in the calculated structures and energies. However, we refrain from speculating on a more detailed model for the observed presence or absence of pentacoordinated isomers in EDTA complexes beyond the calculated energies.

CONCLUSIONS

In summary, we present IR spectra and quantum-chemical calculations on complexes of transition metal dications (Mn, Co, Ni, Cu, and Zn) with EDTA. The IR signatures of the OCO stretching modes of these complexes encode the interactions of the chelated ion with the functional groups of the binding pocket. The complexes are generally found to be in their highest possible spin states, which is an interesting observation, since EDTA has been variously characterized as a strong- or weak-field ligand.[30−32] All are likely to show structures with hexacoordinated metal ions. However, EDTA complexes with Co, Cu, and Zn dications exhibit a substructure in the region of the antisymmetric OCO stretching modes that indicate the presence of additional coordination isomers, particularly with $C = 5$. The electronic structure of the chelated ions affects the contribution of each carboxylate group to the OCO stretching motions in each mode and therefore influences the corresponding IR signatures. The results highlight the variability of EDTA in accommodating ions of different sizes and show how the electronic structure of the guest atom imposes a shape template in the interaction with the EDTA binding pocket.

ASSOCIATED CONTENT

Supporting Information

The Supporting Information is available free of charge at https://pubs.acs.org/doi/10.1021/acs.jpca.2c07996.

> Adiabatic energy gaps; wave function properties of the five lowest eigenstates of $[Mn(II)\cdot EDTA]^{2-}$; frontier natural orbitals of the lowest sextet state of $[Mn(II)\cdot EDTA]^{2-}$; calculated metal−oxygen distances; qualitative amplitude of equatorial and axial OCO oscillators; atomic coordinates of relevant $[M(II)\cdot EDTA]^{2-}$ complexes; calculated modes and intensities for relevant $[M(II)\cdot EDTA]^{2-}$ complexes; relative energies of $[M(II)\cdot EDTA]^{2-}$ isomers in a polarizable continuum; Mulliken charges of metal centers in $[M(II)\cdot EDTA]^{2-}$ complexes; experimental and computed spectra of different isomers of Mn and Ni complexes (PDF)

AUTHOR INFORMATION

Corresponding Author

J. Mathias Weber − *JILA and Department of Chemistry, University of Colorado at Boulder, Boulder, Colorado 80309, United States;* orcid.org/0000-0002-5493-5886; Phone: +1-303-492-7841; Email: weberjm@jila.colorado.edu

Authors

Madison M. Foreman − *JILA and Department of Chemistry, University of Colorado at Boulder, Boulder, Colorado 80309, United States*

Maristella Alessio − *Department of Chemistry, University of Southern California, Los Angeles, California 90089-0482, United States;* orcid.org/0000-0002-0663-5387

Anna I. Krylov − *Department of Chemistry, University of Southern California, Los Angeles, California 90089-0482, United States;* orcid.org/0000-0001-6788-5016

Complete contact information is available at: https://pubs.acs.org/10.1021/acs.jpca.2c07996

Notes

The authors declare no competing financial interest.

ACKNOWLEDGMENTS

J.M.W. gratefully acknowledges support from the U.S. National Science Foundation under award nos. CHE-1764191 and PHY-1734006. This work utilized resources from the University of Colorado Boulder Research Computing Group, which is supported by the National Science Foundation (awards ACI-1532235 and ACI-1532236), the University of Colorado Boulder, and Colorado State University. A.I.K. acknowledges financial support by the U.S. National Science Foundation through the CHE-2154482 grant.

REFERENCES

(1) Vaara, M. Agents That Increase the Permeability of the Outer Membrane. *Microbiol. Rev.* **1992**, *56*, 395−411.

(2) Valeur, B.; Leray, I. Design Principles of Fluorescent Molecular Sensors for Cation Recognition. *Coord. Chem. Rev.* **2000**, *205*, 3−40.

(3) Harrington, J. M.; Boyd, W. A.; Smith, M. V.; Rice, J. R.; Freedman, J. H.; Crumbliss, A. L. Amelioration of Metal-Induced Toxicity in Caenorhabditis Elegans: Utility of Chelating Agents in the Bioremediation of Metals. *Toxicol. Sci.* **2012**, *129*, 49−56.

(4) Waters, S. E.; Robb, B. H.; Marshak, M. P. Effect of Chelation on Iron-Chromium Redox Flow Batteries. *ACS Energy Lett.* **2020**, *5*, 1758−1762.

(5) Burgess, D. R., *National Institute of Standards and Technology. Critically Selected Stability Constants of Metal Complexes. Version 8.0 for Windows*. https://data.nist.gov/od/id/mds2-2154, (accessed Aug 1, 2022).

(6) Louie, A. Y.; Meade, T. J. Metal Complexes as Enzyme Inhibitors. *Chem. Rev.* **1999**, *99*, 2711−2734.

(7) Foreman, M. M.; Weber, J. M. Ion Binding Site Structure and the Role of Water in Alkaline Earth EDTA Complexes. *J. Phys. Chem. Lett.* **2022**, *13*, 8558−8563.

(8) Edington, S. C.; Baiz, C. R. Vibrational Relaxation in EDTA Is Ion-Dependent. *J. Phys. Chem. A* **2018**, *122*, 6585−6592.

(9) Edington, S. C.; Gonzalez, A.; Middendorf, T. R.; Halling, D. B.; Aldrich, R. W.; Baiz, C. R. Coordination to Lanthanide Ions Distorts Binding Site Conformation in Calmodulin. *Proc. Natl. Acad. Sci.* **2018**, *115*, E3126−E3134.

(10) Yuan, Q. Q.; Kong, X. T.; Hou, G. L.; Jiang, L.; Wang, X. B. Photoelectron Spectroscopic and Computational Studies of EDTA·$M(III)^-$ Complexes (M = H_3, Al, Sc, V-Co). *Phys. Chem. Chem. Phys.* **2018**, *20*, 19458−19469.

(11) Yuan, Q. Q.; Kong, X. T.; Hou, G. L.; Jiang, L.; Wang, X. B. Electrospray Ionization Photoelectron Spectroscopy of Cryogenic EDTA·$M(II)^{2-}$ Complexes (M = Ca, V-Zn): Electronic Structures and Intrinsic Redox Properties. *Faraday Disc.* **2019**, *217*, 383−395.

(12) Xu, S.; Gozem, S.; Krylov, A. I.; Christopher, C. R.; Mathias Weber, J. Ligand Influence on the Electronic Spectra of Monocationic Copper-Bipyridine Complexes. *Phys. Chem. Chem. Phys.* **2015**, *17*, 31938−31946.

(13) Foreman, M. M.; Hirsch, R. J.; Weber, J. M. Effects of Formate Binding to a Bipyridine-Based Cobalt-4N Complex. *J. Phys. Chem. A* **2021**, *125*, 7297−7302.
(14) Linstrom, P. J.; Mallard, W. G., Eds., Evaluated Infrared Reference Spectra. In *NIST Chemistry Webbook, NIST Standard Reference Database Number 69*, National Institute of Standards and Technology: Gaithersburg MD, 20899, (accessed May 10, 2022).
(15) Becke, A. D.; Thermochemistry, D.-F. 3. The Role of Exact Exchange. *J. Chem. Phys.* **1993**, *98*, 5648−5652.
(16) Lee, C.; Yang, W.; Parr, R. G. Development of the Colle-Salvetti Correlation-Energy Formula into a Functional of the Electron-Density. *Phys. Rev. B* **1988**, *37*, 785−789.
(17) Shao, Y.; Head-Gordon, M.; Krylov, A. I. The Spin-Flip Approach within Time-Dependent Density Functional Theory: Theory and Applications to Diradicals. *J. Chem. Phys.* **2003**, *118*, 4807−4818.
(18) Chai, J. D.; Head-Gordon, M. Long-Range Corrected Hybrid Density Functionals with Damped Atom-Atom Dispersion Corrections. *Phys. Chem. Chem. Phys.* **2008**, *10*, 6615−6620.
(19) Pokhilko, P.; Epifanovsky, E.; Krylov, A. I. General Framework for Calculating Spin−Orbit Couplings Using Spinless One-Particle Density Matrices: Theory and Application to the Equation-of-Motion Coupled-Cluster Wave Functions. *J. Chem. Phys.* **2019**, *151*, No. 034106.
(20) Mardirossian, N.; Head-Gordon, M. Thirty Years of Density Functional Theory in Computational Chemistry: An Overview and Extensive Assessment of 200 Density Functionals. *Mol. Phys.* **2017**, *115*, 2315−2372.
(21) Weigend, F.; Ahlrichs, R. Balanced Basis Sets of Split Valence, Triple Zeta Valence and Quadruple Zeta Valence Quality for H to Rn: Design and Assessment of Accuracy. *Phys. Chem. Chem. Phys.* **2005**, *7*, 3297−3305.
(22) Epifanovsky, E.; Gilbert, A. T. B.; Feng, X.; Lee, J.; Mao, Y.; Mardirossian, N.; Pokhilko, P.; White, A. F.; Coons, M. P.; Dempwolff, A. L.; et al. Software for the Frontiers of Quantum Chemistry: An Overview of Developments in the Q-Chem 5 Package. *J. Chem. Phys.* **2021**, *155*, No. 084801.
(23) Krylov, A. I.; Gill, P. M. W. Q-Chem: An Engine for Innovation. *WIREs Comput. Mol. Sci.* **2013**, *3*, 317−326.
(24) Bernard, Y. A.; Shao, Y.; Krylov, A. I. General Formulation of Spin-Flip Time-Dependent Density Functional Theory Using Non-Collinear Kernels: Theory, Implementation, and Benchmarks. *J. Chem. Phys.* **2012**, *136*, No. 204103.
(25) Wang, F.; Ziegler, T. Time-Dependent Density Functional Theory Based on a Noncollinear Formulation of the Exchange-Correlation Potential. *J. Chem. Phys.* **2004**, *121*, 12191−12196.
(26) Miertuš, S.; Scrocco, E.; Tomasi, J. Electrostatic Interaction of a Solute with a Continuum. A Direct Utilizaion of Ab Initio Molecular Potentials for the Prevision of Solvent Effects. *Chem. Phys.* **1981**, *55*, 117−129.
(27) Frisch, M. J.; Trucks, G. W.; Schlegel, H. B.; Scuseria, G. E.; Robb, M. A.; Cheeseman, J. R.; Scalmani, G.; Barone, V.; Petersson, G. A.; Nakatsuji, H., et al. *Gaussian 16 Rev. C.01*, Wallingford, CT, 2016.
(28) Cooper, T. E.; O'Brien, J. T.; Williams, E. R.; Armentrout, P. B. Zn^{2+} Has a Primary Hydration Sphere of Five: Ir Action Spectroscopy and Theoretical Studies of Hydrated Zn^{2+} Complexes in the Gas Phase. *J. Phys. Chem. A* **2010**, *114*, 12646−12655.
(29) O'Brien, J. T.; Williams, E. R. Coordination Numbers of Hydrated Divalent Transition Metal Ions Investigated with IRPD Spectroscopy. *J. Phys. Chem. A* **2011**, *115*, 14612−14619.
(30) Kris Krishnan, S. S.; Jervis, R. E. Kinetic Isotopic Exchange Studies of Metal Ion Substitution in EDTA Chelates—I Co(II)-Cobalt (II)-EDTA Exchange. *J. Inorg. Nucl. Chem.* **1967**, *29*, 87−95.
(31) Lati, J. L; Koresh, J.; Meyerstein, D. On the EPR Spectrum of the Trivalent Nickel EDTA Complex in Aqueous Solutions. *Chem. Phys. Lett.* **1975**, *33*, 286−288.
(32) Han, M.; He, J.; Wei, X.; Li, S.; Zhang, C.; Zhang, H.; Sun, W.; Yue, T. Deep Purification of Copper from Cu(II)-EDTA Acidic Wastewater by Fe(III) Replacement/Diethyldithiocarbamate Precipitation. *Chemosphere* **2022**, *300*, No. 134546.

https://doi.org/10.1021/acs.jpca.2c07996
J. Phys. Chem. A 2023, 127, 2258−2264